Improving the Luminescent Properties of Atomic Layer Deposition Eu:Y_2O_3 Thin Films through Optimized Thermal Annealing

Marion Scarafagio, Alexandre Tallaire, Marie-Hélène Chavanne, Michel Cassir, Armelle Ringuedé, Diana Serrano, Philippe Goldner, and Alban Ferrier**

Crystalline rare-earth (RE)-doped Y_2O_3 films are an attractive system for a wide range of photonics applications including quantum technologies which aim at harnessing optical or spin transitions with long coherence times to achieve new functionalities such as quantum storage or information processing. Herein, atomic layer deposition (ALD) of Eu-doped Y_2O_3 thin films with improved optical properties is presented. A crucial post-treatment step to obtain high-quality films is annealing at elevated temperatures (>900 °C). However, the main drawback of this approach is the formation of unwanted parasitic phases due to reaction at the interface with the substrate, especially with silicon. In this article, this issue is discussed for different kinds of substrates and buffer layers. The use of such modified substrates allows advantageously extending the maximum thermal treatment up to 1150 °C without being limited by interface reactions. It is demonstrated that the emission of the $^5D_0 \rightarrow {}^7F_2$ transition for Eu^{3+} in Y_2O_3 film can be as narrow as that of bulk materials when optimized thermal treatments and a thin undoped Y_2O_3 buffer layer are used. Thus, a versatile method to reduce the impact of the substrate–film interface on the optical properties is proposed.

1. Introduction

The development of low-cost, compact, highly integrated optical devices will greatly benefit a large range of applications including optical sensing, telecommunication, spectroscopy, and quantum technologies (QTs). In the framework of QTs, rare-earth (RE)-doped thin films appear as promising systems along other solid-state materials such as NV centers in diamond or quantum dot semiconductors. Indeed, promising results have already been obtained on bulk single crystals as well as on nanoparticles.[1–6] Extremely long spin coherence times (6 h) have, for example, been measured at cryogenic temperatures with Er:Y_2SiO_5 bulk crystals[7] as well as all optical spin coherent control in Eu:Y_2O_3 nanoparticles. In contrast, thin-film technologies are less explored, although they could potentially open the way for on-chip integration with other devices such as light sources or detectors.[8,9] To achieve that, a key requirement is the growth of thin crystalline films of RE-doped oxides with low levels of impurities and defects. In addition, the development of high-quality films can also benefit a broader community because new applications of Y_2O_3 have recently emerged such as catalyst for biodiesel production, wastewater treatment, or anticorrosion.[10–12]

Atomic layer deposition (ALD) enables the deposition of luminescent films with a precise control of thickness at the atomic level. This method relies on exposing the substrate surface alternately to different vaporized precursors until surface self-limiting regime is reached (i.e., an almost complete monolayer of reactant is fully adsorbed at the surface). Due to that sequential approach, ALD allows unique uniform and conformal deposition as well as dopant distribution engineering that prevents concentration quenching even for relatively large doping contents.[13–15] One of the inherent drawbacks of this technique is low growth rates associated with this sequential layer-by-layer growth mode together with low deposition temperatures required to remain within this self-limiting regime (e.g., 50–400 °C).[16,17]

Recently, we demonstrated for RE:Y_2O_3 10 nm thin films that a high deposition temperature and post-treatment annealing above 900 °C are key parameters for optimizing the luminescent properties. In fact, by improving the crystalline environment of the ions, narrow inhomogeneous lines were obtained for the $^7F_0 \leftrightarrow {}^5D_0$ transition of Eu^{3+} even for nanoscale films.[18] Other motivations to work with the cubic structure of Y_2O_3 are the isotropic refractive index and, for Eu^{3+}-doped Y_2O_3, the longest optical and spin coherence lifetime reported for any nanomaterials.[5,6] However, limitations exist. In contrast, deposition temperature cannot be increased easily because it has to remain within the ALD temperature window where the

Dr. M. Scarafagio, Dr. A. Tallaire, M.-H. Chavanne, Prof. M. Cassir, Dr. A. Ringuedé, Dr. D. Serrano, Dr. P. Goldner, Dr. A. Ferrier
Institut de Recherche de Chimie Paris (IRCP)
Université PSL, Chimie ParisTech, CNRS
Paris 75005, France
E-mail: alexandre.tallaire@chimieparistech.psl.eu; alban.ferrier@chimieparistech.psl.eu

Dr. A. Ferrier
Faculté des Sciences et Ingénierie, UFR 933
Sorbonne Universités
Paris 75005, France

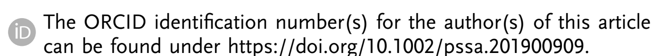
The ORCID identification number(s) for the author(s) of this article can be found under https://doi.org/10.1002/pssa.201900909.

DOI: 10.1002/pssa.201900909

 © 2020 WILEY-VCH Verlag GmbH & Co. KGaA, Weinheim

deposition process is surface limited (temperature range of 250–375 °C for $Y(tmhd)_3$ and O_3 precursors). On the contrary, the annealing post-treatment temperature can only be increased until about 950 °C on silicon above which parasitic silicate phases are formed and modify the emission properties of the RE ions.[18]

In this work, we present strategies to further improve the optical properties of thin $Eu:Y_2O_3$ ALD films and go beyond those limits. First, we investigated the deposition on alternative refractory transparent oxide substrates such as sapphire (Al_2O_3) and yttria (Y_2O_3) transparent ceramics in an attempt to further extend the post-treatment temperature. Another approach is based on the use of buffer layers between the silicon and the luminescent layer. The main idea is to space the reactive interface of silicon from the active $RE:Y_2O_3$ layer. Two different buffer layers were tested: Si_3N_4 or in situ grown undoped Y_2O_3. This approach aims at developing devices compatible with silicon-integrated photonics.[18]

2. Results

RE sesquioxides are polymorphic materials with at least five different crystallographic structures.[19] In the case of Y_2O_3, two main crystal structures are found: a monoclinic (space group C2/m) and a cubic (Ia-3) one.[19,20] Unlike bulk crystals for which the cubic structure is predominant, some competition occurs for nanoscale materials and a monoclinic contribution may be detected. In a previous study, we indeed observed that both phases are deposited by ALD on silicon.[18] The selection during the nucleation between the cubic or the monoclinic structure is complex to predict because it is connected to deposition parameters (temperature and pressure) and to the interaction between the surface and the yttria nuclei. Indeed, a correlation between the surface energy and the polymorphism has been demonstrated for nanocrystals.[20,21] ALD process is expected to be particularly sensitive to the nature of the surface because it is based on self-limited adsorption. Modification of the orientation or the nature of the substrate could lead to texture or the crystallization of new phases in comparison with silicon. To probe the effect of the substrate on the crystalline environment, we used X-ray diffraction (XRD) and photoluminescence (PL) of europium ion transitions. In particular, the $^5D_0 \rightarrow {}^7F_2$ emission is used as a structural probe to distinguish the cubic from the monoclinic phase. Indeed, a narrow line centered at 611 nm is expected for the cubic one, whereas PL is broader and redshifted for the monoclinic structure (centered around 625 nm).[22–24] This large variation is observed because the forced electric dipole (ED) transition $^5D_0 \rightarrow {}^7F_2$ is hypersensitive ($\Delta J = 2$). Those hypersensitive transitions are excellent environment probes because their intensities are much more influenced by the local symmetry around the RE^{3+} ion than the intensities of the other ED transitions.[25,26]

2.1. Deposition on Sapphire Substrates

The main advantages of sapphire in comparison with silicon are the chemical compatibilities of oxide films (e.g., insensitive to oxidation), the transparency, and the lower refractive index (1.77 for sapphire against 1.89 for Y_2O_3 at 600 nm) useful for waveguide technology.[27–29] Furthermore, the higher melting point and thermal stability of sapphire in comparison with silicon implies a lower reactivity. A lower thermal mismatch is also expected because the thermal expansion of Y_2O_3 and Al_2O_3 is close.[30] Among the different Al_2O_3 orientations, we selected the a-plane (11–20) because it shows rectangular symmetry and can be commercially obtained easily.

Figure 1a shows the XRD pattern of 87 nm-thick films doped with 5% Eu^{3+} and grown on a-plane sapphire for different postannealing temperatures. The position of the two main diffraction peaks (222) and (400) is indicated. From the position of the (222) peaks, we calculated a lattice parameter of 10.52 and 10.53 Å for annealing temperatures of 900 and 1000 °C, respectively. This is slightly lower than the expected value for a pure Y_2O_3 ceramic (10.61 Å). For as-grown and low annealing temperatures

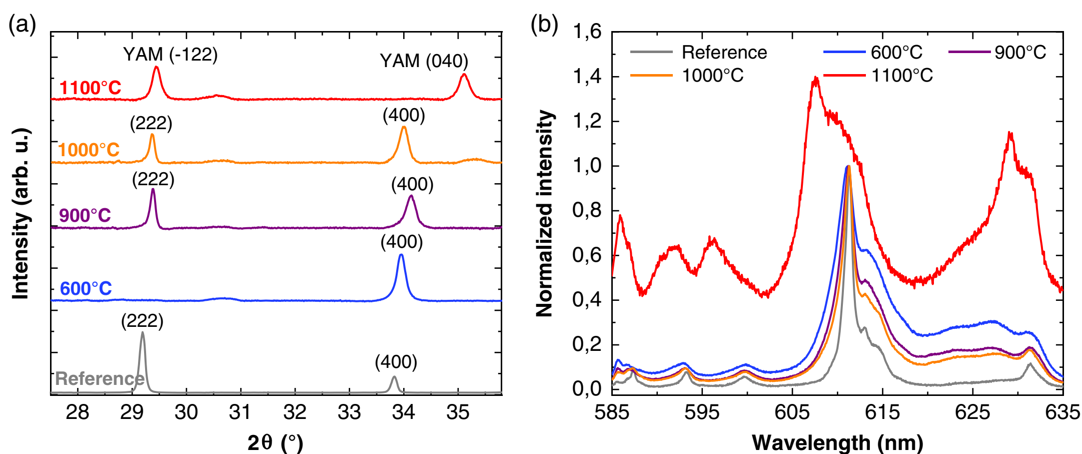

Figure 1. Effect of the annealing temperature on the a) XRD pattern and b) normalized room-temperature PL emission spectra of the $^5D_0 \rightarrow {}^7F_2$ transitions of 87 nm-thick Y_2O_3 films doped with 5% Eu^{3+} and deposited on a-plane Al_2O_3 (11–20) substrates. The XRD data in part (a) are scaled to facilitate comparison. The $Y_4Al_2O_9$ (YAM) peaks present a good agreement with the JCPDS 00-034-0368. The PL spectrum of the sample annealed at 1100 °C (in red) has been vertically translated for better clarity. Nanoparticles and a ceramic with the same composition (in gray) are, respectively, used as references for the XRD pattern and the PL spectra.

© 2020 WILEY-VCH Verlag GmbH & Co. KGaA, Weinheim

(<700 °C), the film is poorly crystallized and preferentially textured along the <100> direction.[18] When the annealing temperature is increased, crystallinity improves and a change in texture occurs because a significant contribution from the (222) planes appears. Other groups have already observed similar changes in orientation during the postannealing treatment.[28,31,32] Until 1000 °C, no additional phases are observed on the XRD pattern. At 1100 °C, the XRD pattern changes significantly and new broad lines become visible, in particular at 29° and 35°. Those new lines are attributed to the monoclinic yttrium aluminate (YAM) $Y_4Al_2O_9$ (JCPDS card 00-034-0368).[33] This indicates that the deposited yttria layer has reacted with the substrate at this temperature and that the ions are located in a different crystalline environment. This solid-state reaction has already been reported for Y_2O_3 sol–gel films deposited on sapphire.[34]

The PL spectra shown in Figure 1b confirm this analysis. In a similar fashion to films on Si substrates, a narrowing of the PL peaks is observed when the annealing temperature increased. The spectra became closer to that measured for a reference transparent ceramic. Furthermore, emission arising from the monoclinic phase of yttria (shown by an arrow in Figure 1b) reduced with an increase in the annealing temperature. When the temperature reached 1100 °C, however, the full width at half maximum (FWHM) increased significantly confirming solid-state reaction with the substrate. A blueshift of the main emission line from 611 to 607 nm suggests the formation of a yttrium–aluminum mixed phase such as Eu:YAM in good agreement with the XRD data.[35] In this phase, Eu^{3+} ions substitute Y^{3+} ions located in a different C_1 symmetry site. This multiplication of substitutional sites together with the lowering of crystal symmetry is responsible for the broadening of the line observed in PL.[36] Therefore, although the use of sapphire as a substrate for Eu:Y_2O_3 thin-film growth allows slightly increasing the maximum annealing temperature compared with a standard Si substrate, a limitation also exists at about 1100 °C due to the formation of parasitic phases.

2.2. Deposition on Y_2O_3 Transparent Ceramics

Undoped Y_2O_3 transparent ceramics have been selected because they have the same composition as the layer and no lattice and thermal mismatch. They may allow limiting stress and interface reactions. The main drawback of this substrate is its noncommercial availability and difficult preparation.[37] The substrates were cut into small pieces of typically $5 \times 5\,mm^2$ and mirror-polished. Structural analysis by XRD does not allow distinguishing signal from the substrate and the layer. For this reason, only PL results are presented. In **Figure 2**, the $^5D_0 \rightarrow {}^7F_2$ PL for different annealing temperatures is shown. For 900 °C annealing and below, an important contribution from the monoclinic phase (indicated by an arrow) is visible showing again that crystallinity remains relatively poor when low annealing temperatures are used. When the annealing temperature is raised above 900 °C, a significant narrowing of the main line at 611 nm is observed. Simultaneously disappearance of the monoclinic contribution occurs. Interestingly in this case, we were able to raise the annealing temperature up to 1200 °C with no obvious limitation by parasitic phases unlike other substrates considered previously.

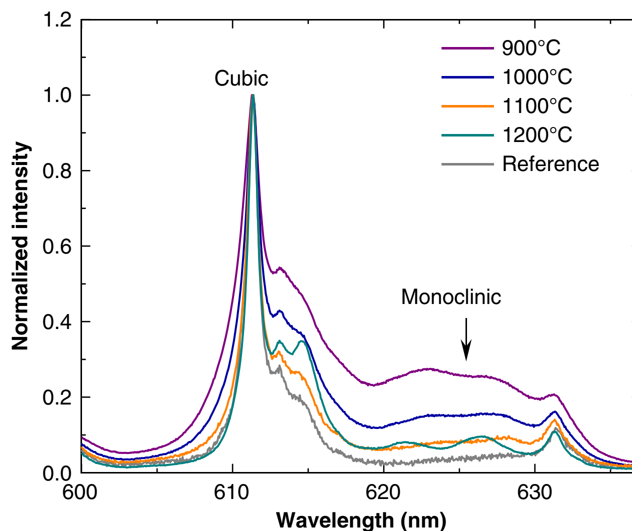

Figure 2. Effect of annealing temperature on the room-temperature PL emission spectra of 82 nm-thick Y_2O_3 films doped with 5% Eu^{3+} and deposited on an undoped Y_2O_3 transparent ceramic. A 5% Eu:Y_2O_3 transparent ceramic is used as a reference (in gray).

At the highest temperature, the PL spectrum is very narrow and the different transitions between Stark sublevels at 622 and 627 nm are resolved. Therefore, the use of such substrates does not present limits in terms of annealing temperatures due to the absence of interfacial reactions. However, one has to consider that diffusion of ions into the bulk ceramic might occur for higher temperatures and longer annealing times.[38] This can be a limiting factor for the foreseen application in QTs for which spatial localization of the emitters in a thin layer at the surface may be required.[39]

Although the transparent ceramic proves to be an ideal candidate for obtaining optimized PL properties of ions in a very high crystalline quality environment, the difficult preparation and poor substrate availability led us to turn to other strategies. In particular, silicon remains an attractive platform with easier scaling-up and postprocessing capabilities. The possibility to limit surface reactions through the intercalation of a buffer layer was thus attempted.

2.3. Deposition on Silicon with a 100 nm-Thick Si_3N_4 Buffer Layer

The first buffer layer studied is a 100 nm-thick low-stress Si_3N_4 deposited on silicon by plasma enhanced chemical vapor deposition (purchased from University Wafer). Deposition of Eu:Y_2O_3 luminescent films has already been reported on Si_3N_4 membrane by e-beam evaporation. Furthermore, Si_3N_4 is a particularly attractive option for capping passivation or buffer layer due to its high barrier properties, low porosity, and high chemical resistance.[40,41] Reactivity between silicon nitride and Y_2O_3 has been largely reviewed because yttria is used as a sintering additive in Si_3N_4 ceramics.[42–44] During the high-temperature sintering process, an intergranular crystalline secondary phase of yttrium silicate such as β-$Y_2Si_2O_7$ was shown to appear at the grain interface of β-Si_3N_4.[42–44]

© 2020 WILEY-VCH Verlag GmbH & Co. KGaA, Weinheim

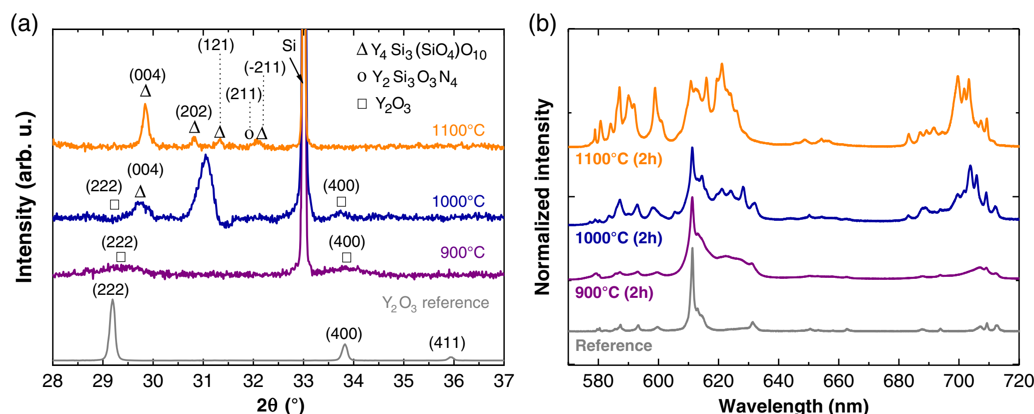

Figure 3. Effect of the annealing temperature on the a) XRD pattern and b) room-temperature PL emission spectra of 100 nm-thick Y_2O_3 films doped with 5% Eu^{3+} and deposited on a Si (100) substrate with a 100 nm buffer layer of Si_3N_4. Nanoparticles and a ceramic with the same composition are, respectively, used as references for the XRD pattern and the PL spectra. The data are scaled to facilitate the comparison. Indexation of the diffraction patterns has been done using the JCPDS 04-015-5862 for $Y_4Si_3(SiO_4)O_{10}$ and 01-086-1105 for $Y_2Si_3O_3N_4$.

The XRD pattern and PL spectra are shown in **Figure 3** for different annealing temperatures. The XRD pattern for the 900 °C annealing presents broad and weak peaks indicating a poor crystalline quality. Furthermore, ratio of the (222) peak area on the (400) one presents a value of about 2, whereas the expected ratio is about 3.6 for a random orientation. The use of Si_3N_4 buffer layer gives a polycrystalline film weakly textured and crystallized. Indeed, the diffraction signal is low and lines are broad, which indicates small crystalline domains. At 1000 °C, a significant change in the XRD pattern occurred with the appearance of new lines possibly related to a reaction with the nitride layer and that are overlapping with that originating from the Y_2O_3 phase. At 1100 °C, indexation of the new lines suggested the presence of two yttrium silicate phases ($Y_4Si_3(SiO_4)O_{10}$ and $Y_2Si_3O_3N_4$) confirming that a solid-state reaction between the silicon substrate, the nitride buffer layer, and the Y_2O_3 layer occurred.

The PL spectra confirm the XRD analysis. Indeed, for a 900 °C annealing post-treatment, the characteristic PL of europium both in the cubic and in the monoclinic phases are present. When the post-treatment annealing rose up to 1000 °C and above, a significant change in the PL spectrum was observed, in a similar way as for a bare silicon wafer, indicating that a reaction occurred between the oxide and the buffer layer or substrate. Therefore, the use of a Si_3N_4 buffer was not sufficient to prevent the formation of parasitic phases.

2.4. Deposition on Silicon with an Undoped Y_2O_3 Buffer Layer

To move away the reactive interface between the substrate and the luminescent layer, we interspaced a Y_2O_3 undoped layer. This 20 nm-thick buffer layer was deposited in situ by ALD before the active luminescent layer of Eu:Y_2O_3. XRD pattern for different annealing temperatures is shown in **Figure 4**. As already observed for deposition on silicon, a strong texture along the <100> direction is observed.[18] The <100> texture remains whatever the annealing temperature, in contrast to growth on sapphire. Furthermore, we observed that the

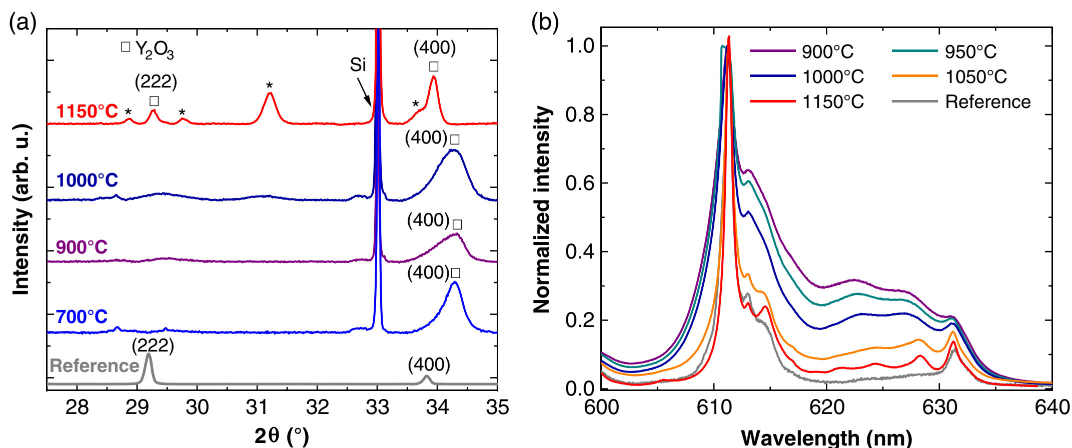

Figure 4. Effect of the annealing temperature on the a) XRD pattern and b) room-temperature PL emission spectra of Y_2O_3 films doped with 5% Eu^{3+} and deposited on a Si (100) substrate with a 20 nm-thick buffer layer of undoped Y_2O_3. Nanoparticles and a ceramic with the same composition are, respectively, used as references for the XRD pattern and the PL spectra. Stars indicate the new XRD peaks due to the formation of the silicate phase.

© 2020 WILEY-VCH Verlag GmbH & Co. KGaA, Weinheim

diffraction peaks are shifted toward higher angles with respect to the reference which suggests the presence of strain as already described by Scarafagio et al.[18] At 1000 °C, a careful analysis of the XRD pattern revealed small additional peaks due to the formation of yttrium silicate compounds. Those new silicate phases (such as Y_2SiO_5 and $Y_2Si_2O_7$) are due to chemical reaction between the Y_2O_3 film and the silicon wafer. For 1150 °C annealing temperature, the intensity of the XRD peaks of the silicate phase increased significantly and is indicated by a star on Figure 4a. On the contrary, no additional lines were observed on the PL spectrum (Figure 4b) even for annealing treatment up to 1100 °C, whereas on a bare silicon wafer (i.e., without the buffer), emission of RE ions would start to be modified at temperatures as low as 1000 °C. In addition, the Stark sublevels were resolved for the highest annealing temperatures. This result indicates that the silicate parasitic phase is well localized at the interface between the silicon wafer and the undoped Y_2O_3 buffer layer but does not extend to the top Eu-doped layer in which the optical properties of the ions are preserved. In this case, the maximum temperature could be increased to values as high as 1150 °C leading to a significant improvement of the crystalline environment.

3. Discussion

Figure 5 and **6** show the effect of the annealing temperature on the PL intensity and area of the $^5D_0 \rightarrow {}^7F_2$ transition for deposition on different substrates. To better visualize the effect, we normalized the data to that collected for a 900 °C annealing. The results are presented up to temperatures at which parasitic phases appear. We can appreciate that the annealing temperature has two effects. For low-temperature annealing (less than 900 °C), a significant increase in the integrated emission (PL area of Figure 5b) is observed by a factor of 5–8. We attribute this larger emission to an increase in the number of Eu^{3+} ions that participate to the PL spectrum. Indeed in this temperature window, the post-treatment annealing is expected to remove quenching centers that would otherwise limit total luminescence emission. This hypothesis has been confirmed for deposition on silicon for which a substantial change in the decay time is observed (data not presented here). Indeed, for as-grown or low-temperature annealed films, the decay time presents a short lifetime with a nonexponential behavior indicating a strong quenching of the europium emission or energy transfer, whereas at higher annealing temperatures the decay time approaches that measured for bulk crystals.[18] It is remarkable on Figure 5b that the PL area remains rather constant when the annealing temperature is further increased. In contrast, the maximum PL intensity continues to rise (Figure 5a). This suggests that crystalline quality improves and that, although the total number of ions contributing to luminescence remains constant, their emission falls within a smaller inhomogeneously broadened line. This is particularly striking for the highest annealing temperatures that show very high PL intensity.

The results are finally shown in Figure 6 which compare the FWHM of the main PL emission at 611 nm for films grown on different substrates. We observe that it strongly decreases with increasing the annealing temperature until the maximum temperature of formation of parasitic phases (silicate or aluminate) is reached. Both depositions on the Y_2O_3 buffered substrate and the transparent ceramic allow advantageously extending the post-treatment to more than 1100 °C without encountering this issue. This translates into much narrower PL linewidths that are comparable or even improved with respect to the reference bulk ceramic material.

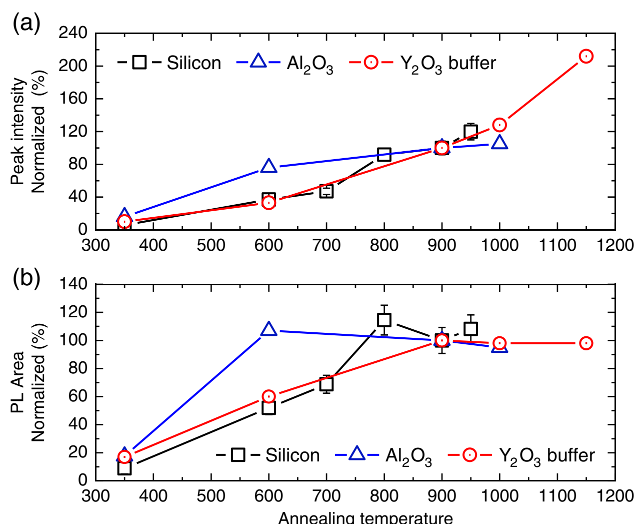

Figure 5. Comparison of the $^5D_0 \rightarrow {}^7F_2$ PL for films deposited on silicon, on Al_2O_3 (11–20), and silicon with a 20 nm-thick Y_2O_3 buffer layer. a) Comparison of the variation of the normalized integrated PL signal in the range of 580–640 nm as a function of the annealing temperature. b) Variation of the normalized 611 nm peak intensity for different annealing temperatures. For each substrate, the values of the PL area and PL peak intensity were normalized to that obtained for a 900 °C annealing.

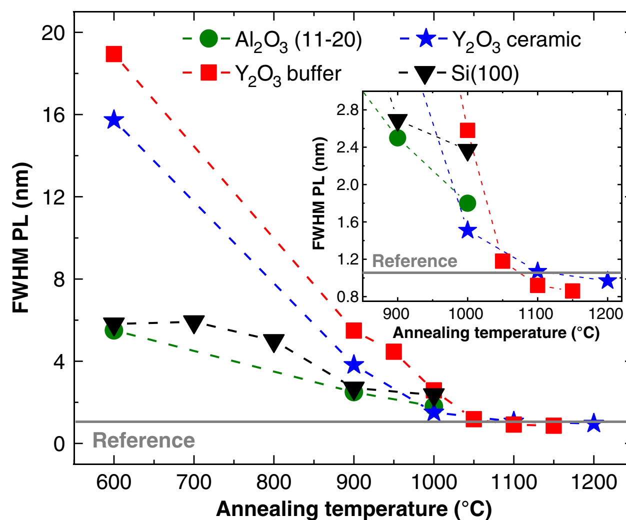

Figure 6. Comparison of the FWHM of the $^5D_0 \rightarrow {}^7F_2$ red emission of $Eu:Y_2O_3$ as a function of the annealing temperature. A drastic decrease in the FWHM is observed when the annealing temperature is increased. The inset represents a zoom into the high-temperature area (850–1250 °C). The reference value is measured on a transparent ceramic of the same composition.

© 2020 WILEY-VCH Verlag GmbH & Co. KGaA, Weinheim

4. Conclusion

In this work, we fabricated Eu^{3+}-doped Y_2O_3 thin films on different substrates by ALD and compared the structural and PL properties with standard deposition on Si (100). For all the substrates, crystalline films were obtained exemplifying the great versatility of the ALD deposition technique. To maximize the PL intensity, a high-temperature annealing post-treatment enhancement is required but the appearance of parasitic interfacial phases is usually a strong limiting factor. For the growth on Al_2O_3 substrates, the maximum annealing temperature is slightly improved (1050 °C) compared with that of bare silicon (950 °C). Furthermore, the use of a buffer layer such as Si_3N_4 did not help in increasing this temperature. When a transparent ceramic is used as a substrate, no interfacial reactions are formed allowing extending post-treatment up to 1200 °C. We note though that diffusion of the dopants deep into the matrix might occur and could be an issue for QT applications for which localized dopants are needed. Given the difficulty of preparation and poor availability of the material, transparent Y_2O_3 ceramics also do not constitute an ideal platform. The use of a thin undoped Y_2O_3 buffer layer was found to be the most appealing strategy allowing annealing up to 1150 °C without modifying Eu^{3+} PL on the top Eu-doped active layer, whereas significant changes in the XRD pattern were observed. This suggests that this thin layer acted as a sacrificial interface that reacted with the silicon substrate and prevented the development of the silicate parasitic phase further into the Eu-doped film. The use of this approach of sacrificial undoped layer is a versatile method that could be applied to other photonics systems.

5. Experimental Section

Film depositions were conducted with a Picosun Sunale R200 using conventional β-diketonate precursors: $Y(tmhd)_3$ and $Eu(tmhd)_3$ from (99.9%, Strem Chemicals). These stable precursors were held at 140–160 °C and delivered using 300 sccm N_2 carrier gas. The vaporized precursors were sent sequentially with an oxidant gas (O_3) into the thermalized deposition chamber at 300–350 °C. To maximize the film crystallinity, we used ozone as a strong oxidizing agent. A typical ALD sequence consisted of a 3 s $Y(tmhd)_3$ pulse followed by a 3 s purging pulse of N_2; a 3 s ozone pulse also followed by a 3 s purge with N_2. Eu doping of the oxide films was easily tuned by sequentially introducing pulses of the dopant element in the standard yttrium oxide cycle. In our case, a doping level of 5% was used by introducing five pulses of $Eu(tmhd)_3$ every 95 pulses of $Y(tmhd)_3$. More details about the impact of the different deposition parameters and their optimization were discussed in details in Scarafagio et al.[18]

The following different substrates were considered for deposition: silicon (100), a-plane Al_2O_3 sapphire (11–20), Y_2O_3 transparent ceramic and low thermal stress 100 nm-thick Si_3N_4 deposited on Si(100). All substrates were used as received after cleaning with ethanol, acetone with ultrasonic bath. They were all purchased from private companies except for the Y_2O_3 ceramics that were provided by Dr Ikesue (World Lab Co., Nagoya, Japan). To remove experimental bias, deposition on a reference silicon (100) wafer was done for systematic comparison for each experiment. To improve the crystallinity of the films and the optical properties of the emitters, we investigated a postgrowth annealing treatment at different temperatures in air for 2 h. The crystallinity of the films was evaluated using XRD with a Panalytical X'Pert Pro diffractometer using an incident beam Ge monochromator, and a stainless-steel sample holder. For all XRD patterns, baseline from *Fullprof* software was subtracted.

Film thickness was measured by white light interferometry in the range of 250–1000 nm with an Ocean Optics NanoCalc system using Y_2O_3 optical constants. Finally, PL measurements were performed in a Renishaw InVia micro-PL apparatus with a 50× objective and a 532 nm laser as the excitation source.

Acknowledgements

This project has received funding from the European Union's Horizon 2020 research and innovation program under grant agreement no. 712721 (NanOQTech) and from Région Ile de France through the SIRTEQ framework. The authors thank Dr. Ikesue for providing transparent ceramic samples.

Conflict of Interest

The authors declare no conflict of interest.

Keywords

atomic layer deposition, lanthanide, photoluminescence, quantum technologies, sesquioxide

Received: November 5, 2019
Revised: January 17, 2020
Published online:

[1] P. Goldner, A. Ferrier, O. Guillot-Noël, *Handb. Phys. Chem. Rare Earths* **2015**, *46*, 1.
[2] F. Bussières, C. Clausen, A. Tiranov, B. Korzh, V. B. Verma, S. W. Nam, F. Marsili, A. Ferrier, P. Goldner, H. Herrmann, C. Silberhorn, W. Sohler, M. Afzelius, N. Gisin, *Nat. Photonics* **2014**, *8*, 775.
[3] A. Perrot, P. Goldner, D. Giaume, M. Lovrić, C. Andriamiadamanana, R. R. Gonçalves, *Phys. Rev. Lett.* **2013**, *111*, 203601.
[4] J. G. Bartholomew, K. de Oliveira Lima, A. Ferrier, P. Goldner, *Nano Lett.* **2017**, *17*, 778.
[5] S. Liu, D. Serrano, A. Fossati, A. Tallaire, A. Ferrier, P. Goldner, *RSC Adv.* **2018**, *8*, 37098.
[6] D. Serrano, J. Karlsson, A. Fossati, A. Ferrier, P. Goldner, *Nat. Commun.* **2018**, *9*, 2127.
[7] M. Zhong, M. P. Hedges, R. L. Ahlefeldt, J. G. Bartholomew, S. E. Beavan, S. M. Wittig, J. J. Longdell, M. Sellars, *Nature* **2015**, *517*, 177.
[8] K. J. Tielrooij, L. Orona, A. Ferrier, M. Badioli, G. Navickaite, S. Coop, S. Nanot, B. Kalinic, T. Cesca, L. Gaudreau, Q. Ma, *Nat. Phys.* **2015**, *11*, 281.
[9] J. H. Kang, H.-D. Yang, B. S. Joo, J.-S. Park, S.-E. Lee, S. Jeong, J. Kyhm, M. Han, J. D. Song, I. K. Han, *Opt. Express* **2017**, *25*, 19561.
[10] P. Zhang, *Catal. Lett.* **2019**, *149*, 2433.
[11] S. Lee, K. Matsuda, M. Tanaka, T. Tsuchiya, K. Nishimura, Y. Hishinuma, T. Tanaka, T. Muroga, *Thin Solid Films* **2019**, *689*, 137455.
[12] G. Azimi, R. Dhiman, H.-M. Kwon, A. T. Paxson, K. K. Varanasi, *Nat. Mater.* **2013**, *12*, 315.
[13] J. Rönn, L. Karvonen, C. Kauppinen, A. Pyymaki Perros, N. Peyghambarian, H. Lipsanen, A. Saynatjoki, Z. Sun, *ACS Photonics* **2016**, *3*, 2040.
[14] T. Proslier, N. G. Becker, M. J. Pellin, J. Klug, J. W. Elam, *US Patent 8518179 B1* **2013**.

© 2020 WILEY-VCH Verlag GmbH & Co. KGaA, Weinheim

[15] T. T. Van, J. P. Chang, *Appl. Phys. Lett.* **2005**, *87*, 011907.
[16] M. Fanciulli, G. Scarel, *Rare Earth Oxide Thin Films*, Springer Series in Topics in Applied Science, Springer, Berlin, Heidelberg **2007**, pp. 203–223.
[17] M. Leskelä, M. Ritala, *Angew. Chem., Int. Ed. Engl.* **2003**, *42*, 5548.
[18] M. Scarafagio, A. Tallaire, K.-J. Tielrooij, D. Cano, A. Grishin, M.-H. Chavanne, F. H. L. Koppens, A. Ringuedé, M. Cassir, D. Serrano, P. Goldner, A. Ferrier, *J. Phys. Chem. C* **2019**, *123*, 13354.
[19] G.-Y. Adachi, N. Imanaka, *Chem. Rev.* **1998**, *98*, 1479.
[20] B. Guo, Z. P. Luo, *J. Am. Ceram. Soc.* **2008**, *91*, 1653.
[21] A. Navrotsky, *Geochem. Trans.* **2003**, *4*, 34.
[22] D. K. Williams, B. Bihari, B. M. Tissue, J. M. McHale, *J. Phys. Chem. B* **1998**, *102*, 916.
[23] J. Zhang, H. Cui, P. Zhu, C. Ma, X. Wu, H. Zhu, Y. Ma, Q. Cui, *J. Appl. Phys.* **2014**, *115*, 023502.
[24] Y. C. Kang, D. J. Seo, S. B. Park, H. D. Park, *Jpn. J. Appl. Phys* **2001**, *40*, 4083.
[25] K. Binnemans, *Coord. Chem. Rev.* **2015**, *295*, 1.
[26] F. S. Richardson, *Chem. Rev.* **1982**, *82*, 541.
[27] M. B. Korzenski, P. Lecoeur, B. Mercey, D. Chippaux, B. Raveau, R. Desfeux, *Chem. Mater.* **2000**, *12*, 3139.
[28] M. B. Korzenski, P. Lecoeur, B. Mercey, P. Camy, J. L. Doualan, *Appl. Phys. Lett.* **2001**, *78*, 9.
[29] C. Grivas, R. W. Eason, *J. Phys.: Condens. Matter* **2008**, *20*, 264011.
[30] P. Mechnich, W. Braue, *J. Eur. Ceram. Soc.* **2013**, *33*, 2645.
[31] F. Jollet, C. Noguera, M. Gautier, N. Thromat, J. P. Duraud, *J. Am. Ceram. Soc.* **1991**, *74*, 358.
[32] C. W. Nieh, Y. J. Lee, W. C. Lee, Z. K. Yang, A. R. Kortan, M. Hong, J. Kwo, C.-H. Hsu, *Appl. Phys. Lett.* **2008**, *92*, 061914.
[33] S. Arakawa, H. Kadoura, T. Uyama, K. Takatori, Y. Takeda, T. Tani, *J. Eur. Ceram. Soc.* **2016**, *36*, 663.
[34] J. Y. Cho, K.-Y. Ko, Y. R. Do, *Thin Solid Films* **2007**, *515*, 3373.
[35] H. C. Jung, J. Y. Park, G. S. Rama Raju, J. H. Jeong, B. K. Moon, J. H. Kim, H. Y. Choi, *Curr. Appl. Phys.* **2009**, *9*, S217.
[36] M. Kaczkan, S. Turczynski, D. A. Pawlak, M. Wencka, M. Malinowski, *Opt. Mater.* **2016**, *58*, 412.
[37] A. Ikesue, Y. L. Aung, *Nat. Photonics* **2008**, *2*, 721.
[38] S. R. Podowitz, R. Gaumé, R. S. Feigelson, *J. Am. Ceram. Soc.* **2010**, *93*, 82.
[39] T. Kornher, K. Xia, R. Kolesov, N. Kukharchyk, R. Reuter, P. Siyushev, R. Stöhr, M. Schreck, H.-W. Becker, B. Villa, A. D. Wieck, Wrachtrup, *J. Appl. Phys. Lett.* **2016**, *108*, 053108.
[40] E. Vanhove, A. Tsopela, L. Bouscayrol, A. Desmoulin, J. Launay, *Sens. Actuators B* **2013**, *178*, 350.
[41] Y. Tshuchiya, M. Endoh, M. Kurosawa, R. T. Tung, T. Hattiri, S. Oda, *Jpn. J. Appl. Phys.* **2003**, *42*, 1957.
[42] M. K. Cinibulk, G. Thomas, *J. Am. Ceram. Soc.* **1992**, *75*, 2037.
[43] T. Honma, Y. Ukyo, *J. Mater. Sci. Lett.* **1999**, *18*, 735.
[44] H.-H. Lu, J.-L. Huang, *Ceram. Int.* **2001**, *27*, 621.

© 2020 WILEY-VCH Verlag GmbH & Co. KGaA, Weinheim